PCCP

PAPER

View Article Online
View Journal | View Issue

Cite this: *Phys. Chem. Chem. Phys.*, 2023, **25**, 27293

Synthesis and composition modification of precipitate tubes in a confined flow reactor†

Kinga Bene,‡ Edina Balog‡ and Gábor Schuszter *

Received 21st July 2023,
Accepted 13th September 2023

DOI: 10.1039/d3cp03467d

rsc.li/pccp

Precipitation reactions coupled to various transport phenomena, such as flow or diffusion, lead to the formation of different spatial gradients which can be influenced by tuning the experimental parameters (*e.g.*, reactant concentration, flow rate, reactor geometry, *etc.*). Thereby it gives us the opportunity to change the micro and macrostructure of the products. Herein, we investigate the precipitate tube formation in a flow-driven system applying a horizontal confined geometry for individual and composite alkaline earth metal (Mg(II), Ca(II), Sr(II), and Ba(II))–carbonate systems. First we attempted to achieve tube-like structures in each reactive system by increasing the reactant concentrations. It is found that the precipitate tubes are not present in the magnesium–carbonate system even at extremely high concentrations. Therefore, we doped the magnesium solution with other alkaline earth metal ions, which resulted in the desired precipitate patterns. Besides the macroscopic characteristics, the microstructure of the crystals (morphology, crystal phase, size, and composition) could also be modified by combining the ions and varying their concentration ratio. In addition, by varying the relative concentration of the alkaline earth metal cations, separated and composite crystals could also be produced as different extrema. These were spatially isolated due to the reactor geometry, and thus the products, which contain the metal ions either homogeneously or individually, can be easily separated from each other.

1 Introduction

The most generally known precipitate tube structure is the 3-dimensional chemical garden, in which plant-like patterns form as a result of the reaction between various metal salt crystals and sodium silicate solution.[1] In the growth of these tubes the osmotic effects and buoyancy play an important role. However, in these systems the growth direction and the diameter of tubes are stochastic and the composition of products is not controllable. In order to gain a better regulation on tube formation, the precipitation reaction has been coupled with flow, which allows controlled growth and adjustable composition.[2–5] Besides the simple injection process, there are various methods which can influence the quality of the forming tubes such as bubble guidance,[6,7] and growth in the cation-exchange membrane[8,9] or in gel medium.[10,11]

Haudin *et al.* have presented the chemical garden pattern formation in a quasi two dimensional horizontal confined flow reactor (so-called Hele–Shaw cell) by applying the reactions of different metal ions with silicate solution.[12] By comparing the macroscopic precipitate tube structures, it was observed that the chemical nature of the reactants does not play a key role in the tube growth at extremely high concentrations and flow rates. However, by utilizing similar confined flow reactors and moderate experimental conditions, numerous examples have been presented in the literature in which the characteristics of precipitate patterns depend on the applied chemical system.[13–15] Based on these results, in our previous work we examined the causes of the precipitate tube formation in various chemical systems. We pinpointed experimental parameters, under which patterns of some chemical systems show isotropic growth by applying a radial injection, while others show directed growth of precipitate membranes and tube structures. This phenomenon was explained by the microstructure of the forming crystals. If a low number of large particles build up the pattern, the spatial distribution of the particles is homogeneous on a macroscopic scale. In contrast, when a large number of small particles form during the reaction, a membrane-like precipitate pattern evolves. The reason for this is the van der Waals interaction between the small particles, which results in a colloidal gel between the reactant solutions. This gel locally generates a large viscosity gradient. As a result, upon injection, a phenomenon analogous to viscous fingering causes the formation of the membrane and/or tube-like structure of the precipitate patterns.[16,17] This membrane formation is more pronounced at high reactant concentrations, because

Department of Physical Chemistry and Materials Science, University of Szeged, Rerrich Béla tér 1, Szeged, H-6720, Hungary. E-mail: schuszti@chem.u-szeged.hu

† Electronic supplementary information (ESI) available. See DOI: https://doi.org/10.1039/d3cp03467d

‡ These authors contributed equally to the work.

high supersaturation favors nucleation rather than crystal growth.[18]

Considering these previous results, in this work our goal was the designed production of precipitate tubes in a flow-driven system and confined geometry, in the case of various alkaline earth metal–carbonate precipitation systems. In the first step, we attempted to achieve the membrane-like structure by increasing the concentration of single metal ion (Mg(II), Ca(II), Sr(II), or Ba(II)) solutions. Although the tubes were not present in the magnesium–carbonate system even at high supersaturation, other alkaline earth metals showed tube formation with a tendency to increase down the periodic table. In the next step we added various alkaline earth metals at different concentrations into a magnesium chloride reactant solution in order to favor nucleation. This composite system resulted in a precipitate tube structure, and furthermore, it enabled the composition modification of the forming tubes. During the microstructure analysis it was revealed that by combining the metal ions we can vary the morphology and crystalline phase compared to the individual systems, and by fine-tuning the initial concentration ratio, crystals with different sizes and compositions (well-separated and/or composite crystals) can also be obtained.

2. Experimental

The flow-driven experiments were carried out in a horizontal confined geometry shaped between a large lower pool (35 × 35 cm^2) and a smaller upper plate (21 × 21 cm^2) made of Plexiglas (8 mm thickness) which is known as a Hele–Shaw cell (Fig. 1a).

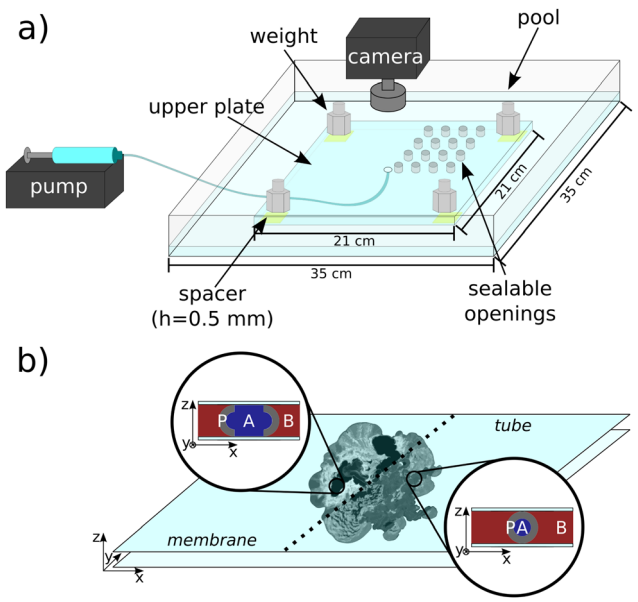

Fig. 1 Schematics of the experimental setup: Horizontally oriented Plexiglas Hele–Shaw cell (a). Schematics of the membrane- and tube-like structures evolving in the confined flow reactor (b). A (blue): Injected sodium carbonate solution; B (red): displaced alkaline earth metal solution; P (grey): reaction product.

The layer thickness of 0.5 mm between the two Plexiglas plates was maintained by four spacers and four weights, which were placed below the corners of the upper plate. The experimental setup was illuminated from the two sides by lamps and a grayscale digital camera (Unibrain Compact Firewire-400) was placed above the reactor to record the dynamics of the reactions. In the thin horizontal gap, the host alkaline earth metal aqueous solutions (chemicals used: $MgCl_2{\cdot}6H_2O$, $CaCl_2{\cdot}2H_2O$, $SrCl_2{\cdot}6H_2O$, $BaCl_2{\cdot}2H_2O$) and their concentrations (0.25–1.5 M) were varied in the case of different experiments. We applied the displaced solutions in this concentration range because a relatively high concentration (0.25 M) was necessary in order to produce macroscopically visible precipitate patterns, and we could prepare solution from $BaCl_2{\cdot}2H_2O$ of up to 1.53 M due to its solubility. To ensure the homogeneous outflow of the solution, the same host solution was poured into the pool around the upper plate to form a buffer liquid layer of approx. 4 mm depth. In each experiment, 5 mL aqueous sodium carbonate solution (Na_2CO_3, 1.5 M) was injected into the gap with Q = 1 mL min^{-1} flow rate from the center of the lower pool through a hole with a diameter of 1 mm by utilizing a syringe pump (KDS-210 P-CE).

If a large number of small crystals evolve as a result of the reaction taking place in the Hele–Shaw cell (Fig. 1a), van der Waals interactions will be present between the particles. Due to this, a membrane- and/or tube-like structure can form, the difference between the two structures is shown in Fig. 1b. In case of the membrane structure, there is an open area between the precipitate walls which separate the reactant solutions. In contrast, the tube structure forms when the precipitate wall completely surrounds the injected reactant solution. During our work, in order to produce membrane-like precipitate structures (Fig. 1b) in the case of magnesium–carbonate system, calcium, strontium, or barium ions with different concentrations (0.25–1.5 M) were also added into 1.5 M magnesium(II) solution. This mixed host solution was filled in between the two Plexiglas plates prior to the injection experiment.

The microstructure analysis of the forming crystals was carried out using a scanning electron microscope connected to an energy dispersive X-ray spectroscope (SEM with EDX, Hitachi S4700). During the SEM analysis, the samples were coated with a thin gold layer and we used a 10 kV accelerating voltage; accelerating voltage was 20 kV for EDX measurements. In order to gain information about the crystalline phase, the samples were examined by a powder X-ray diffractometer (PXRD, Rigaku MiniFlex II Desktop X-ray diffractometer) as well, with CuKα (= 0.1542 nm) as a radiation source in the 2θ = 15–70° range applying 0.02° step size and 4° min^{-1} scan speed. For the microstructure and crystalline phase analysis we had to take samples from the corresponding regions of the macroscopic precipitate patterns. However, when the upper plate of the reactor is lifted, the patterns are destroyed as a result of the surface tension, and the leftover of the reactant solutions continues to mix and react. Because of the latter, we could not distinguish the crystals which appeared due to this mixing from those that formed during the injection. To eliminate this effect, we designed an upper plate to facilitate the precision

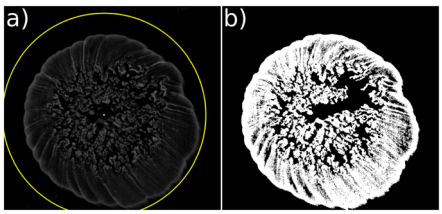

Fig. 2 Computer reconstructed image of the pattern (a) for the determination of integrated light intensity of the image (I) and that of precipitate area (A, b). c_{CaCl_2} = 0.5 M, $c_{Na_2CO_3}$ = 1.5 M, Q = 1 mL min^{-1}, $V_{Na_2CO_3}$ = 5 mL.

sampling method (Fig. 1a). This upper plate was also made of Plexiglas, but we drilled 4 × 4 pieces of small (1.5 cm diameter), systematically positioned and sealable openings (the distance between the openings is 1 cm) on the lid. Our preliminary experiments proved that these holes in closed position do not affect the flow field; however, they enable precise sampling at the end of the reaction. The sampling was carried out by using an automatic pipette, then the sample was placed into an Eppendorf tube. The sedimentation of the precipitate taken from the pattern was enhanced by using a centrifuge (Eppendorf AG 22331 Hamburg). Finally, the precipitate was washed 2–3 times with distilled water and allowed to dry at ambient temperature.

In order to gain information about the amount of precipitate, the semi-quantitative analysis of the 2-dimensional macroscopic patterns was carried out using a Wolfram Mathematica algorithm. To distinguish the precipitate from the background in the recorded images, a threshold value was set in the program. Where the pixel was brighter than this threshold the program counted it as precipitate, while the darker parts of the picture were not taken into account. Fig. 2a shows a computer reconstructed image of the pattern. The area covered by precipitate particles (A, Fig. 2b) was sought.[14] The change of the amount of precipitate was estimated based on the integrated intensity (I) of the images. Higher intensity means greater amount of precipitate; however, exact quantitative analysis is not possible due to the different refractive index of the precipitates obtained in the different chemical systems.

3. Results and discussion

3.1 Macroscopic precipitate patterns

3.1.1 One component carbonate precipitates. In this work we examined the pattern formation of carbonate precipitates of different alkaline earth metals. During the experiments, a constant volume of sodium carbonate solution (5 mL, 1.5 M) was injected in the magnesium, calcium, strontium or barium ion containing host solution. The concentration of the host solution was varied (0.25–1.5 M), but the flow rate was constant (Q = 1 mL min^{-1}). Thanks to the different densities of the host and injected solutions, convective mixing takes place between the reactants from the beginning of the injection. Due to the supersaturation in the mixing zone of the displaced and injected solutions, precipitate formation is observed. The interaction between the precipitation reaction and hydrodynamics leads to the formation of different precipitate patterns, whose characteristics significantly depend on the applied experimental parameters. Under the given conditions, each experiment was reproduced three times to draw reliable conclusions.

Fig. 3 shows the macroscopic precipitation patterns of the various alkaline earth metal–carbonate systems. We applied different cation concentrations in order to find out which is the lowest concentration necessary in order to reach the membrane and/or tube structure (see Fig. 1b). In the case of constant flow rate and cation concentration, it is observed that, as the mass number of the alkaline earth metal increases, the amount of precipitate and therefore the coverage of the pattern increases (grayscale intensity (I) and precipitate covered area (A) values in the 0.25 M column of Fig. 3). The cause of this is that, from magnesium–carbonate to barium–carbonate system, the reactions are faster[19] and the forming crystals become larger and heavier,[14] thus they sediment earlier. The precipitate occupies a large area inside the periphery of the patterns, which results in a greater value of A. In addition, the solubility product of carbonate precipitates decreases towards the barium carbonate (pK_{sp} values given later); consequently, the solubility of this precipitate is the lowest of all products, which means a larger value of I. We can also see in Fig. 3 that at lower concentrations there is a larger precipitate-free area in the middle of the patterns which, in the case of the magnesium–carbonate system, is significant even at higher concentrations. The crystals, which build up the precipitate pattern, are too small and sediment later, as previously described. In addition, this reaction is slow compared to other alkaline earth metal–carbonate systems, thus the crystals appear later compared to the timescale of the flow. Due to this, the membrane-like structure, and thus the tubes do not evolve in the magnesium system. In contrast, if the concentration of the metal ion increases in the case of calcium, strontium, and barium carbonate, the change in the characteristics of the pattern is significant. In the case of calcium–carbonate system, by using the most concentrated solutions, a membrane-like structure formed (serpentine precipitate structure with distinct walls and an open area between them; Fig. 3, $CaCl_2$ row, 1.5 M concentration). The membrane-like structure became even more pronounced in the strontium- and barium–carbonate systems (last column of Fig. 3). The precipitate membrane appeared immediately after the contact of the reactant solutions and precipitate tubes (3-dimensional membranes, *i.e.*, closed precipitate tubes) could form at 1.5 M strontium chloride and 1.0 M barium chloride concentration. The reason for the membrane formation is the increased supersaturation caused by the high concentration of the reactants compared to the previous columns of Fig. 3. These experimental conditions favor nucleation, which results in the tube structure in agreement with the literature.[16] Our results also show that, by going down in the periodic table of the elements, the tube structure appears at lower and lower concentrations. According to this, in the case of calcium–carbonate system, a further increase of concentration would

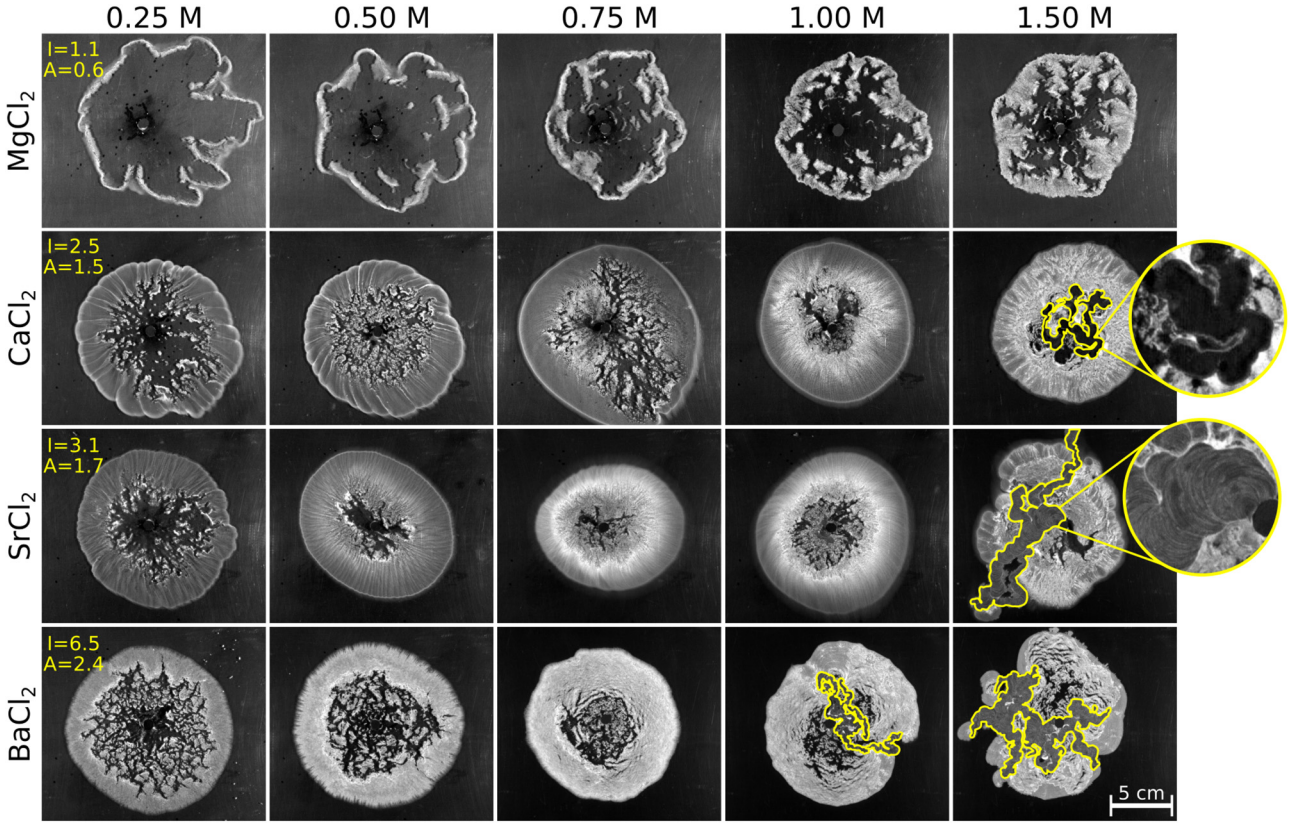

Fig. 3 Macroscopic patterns of alkaline earth metal–carbonate precipitation systems at different alkaline earth metal concentrations. The precipitate membrane and/or tube structure is marked with yellow (Fig. S1 shows the original images of the patterns without the color marking, ESI†). The grayscale intensity ($I/10^4$ a.u.) and the precipitate covered area ($A/10^5$ px^2) values are marked in 0.25 M column; the standard deviation of the values is about 15% in each case. The enlarged images show the difference between the precipitate membrane and tube structures; see the text for further explanation. $c_{Na_2CO_3}$ = 1.5 M; Q = 1 mL min^{-1}; $V_{Na_2CO_3}$ = 5 mL.

probably lead to the formation of a more pronounced precipitate tube structure.

3.1.2 Two component carbonate precipitates. In this work our aim was to produce precipitate tubes in alkaline earth

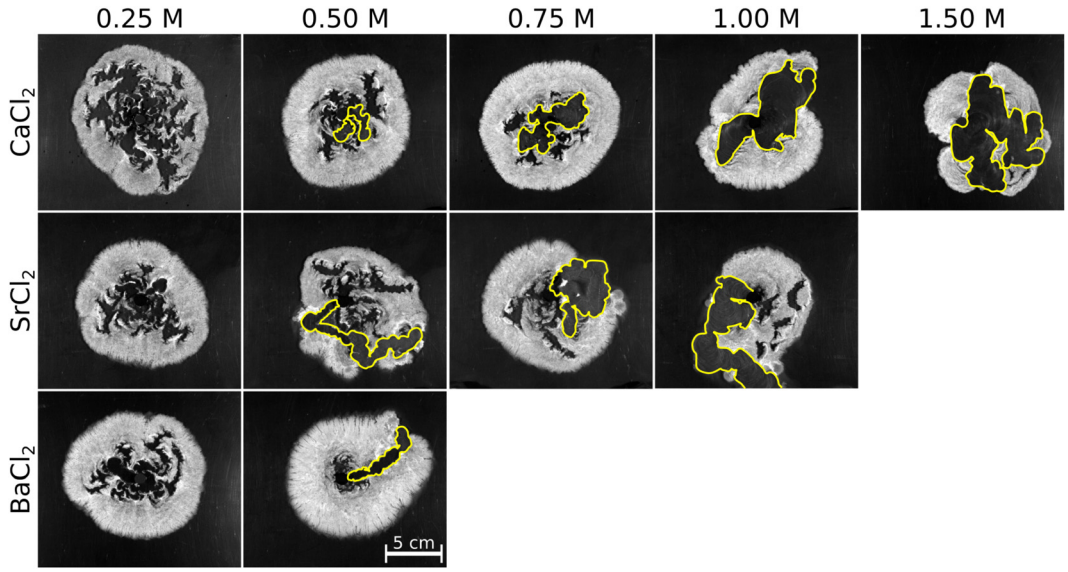

Fig. 4 Macroscopic precipitate tubes produced by the addition of alkaline earth metal ions in different concentrations into a magnesium chloride solution. The precipitate membrane structure is marked with yellow. $c_{Na_2CO_3}$ = 1.5 M; c_{MgCl_2} = 1.5 M; Q = 1 mL min^{-1}; $V_{Na_2CO_3}$ = 5 mL.

metal–carbonate systems and modify their composition in a 2-dimensional reactor. In the case of the magnesium–carbonate system, the membrane-like structure did not evolve even at the highest concentration as shown in Fig. 3. Therefore, we attempted to achieve the precipitate membrane and/or tube structure in the magnesium–carbonate system by favoring the process of nucleation and by increasing the degree of supersaturation. In order to do this, calcium, strontium, and barium chlorides were added separately and in different concentrations (0.25–1.5 M) to a magnesium chloride solution (1.5 M) and then the sodium carbonate solution (1.5 M) was injected into these host solutions. The added salts are not only significant because they increase the supersaturation, but they are characterized by faster precipitate formation compared to the magnesium–carbonate system.[20] Because of this, the nucleation process of magnesium containing precipitate could be accelerated by heterogeneous nucleation, for example, by the formation of magnesium precipitates on tiny calcium carbonate crystals. In the concentrated magnesium chloride solution (1.5 M) we could dissolve the strontium chloride up to 1 M, while the barium chloride up to 0.5 M. Fig. 4 shows the macroscopic precipitate patterns when the other alkaline earth metal was added to the magnesium(II) solution in different concentrations. It is observed that the formation of precipitate membrane and/or tube structure is present already at small cation dosage (0.5 M). Similarly to the individual systems, as we go down in the periodic table of the elements, the tube formation becomes more pronounced as shown by the growing size of the tube pattern. In addition, if we increase the concentration of the added alkaline earth metal cation, the tubes become wider because the nucleation is rapid and the membrane structure is completely dominant. In the magnesium-free systems, we had to use higher concentrations to achieve the same structure (1.5 M for calcium and strontium, and 1.0 M for barium). The added calcium, strontium, and barium ions not only make the nucleation faster compared to the pure magnesium system, but the composite system also shows enhanced nucleation compared to all individual systems. Due to this fast nucleation we assumed that magnesium and the other alkaline earth metal precipitates build up together the 3-dimensional tubes. Later in the manuscript we will address this assumption.

The macroscopic precipitate patterns were quantitatively analyzed by image processing. The systems which contained calcium ion were chosen as reference, because we could add this alkaline earth metal at the highest concentration to the 1.5 M magnesium chloride solution. The graph in Fig. S2 (ESI†) illustrates the dependence of picture grayscale intensity (I) and precipitate covered area (A) values as a function of calcium chloride concentration. In the case of the pure calcium–carbonate system, the intensity of patterns, and thus the amount of precipitate increases monotonically with increasing calcium ion concentration. The precipitate covered area also grows with calcium ion concentration. A higher calcium ion concentration causes a faster reaction, thus the crystals precipitate immediately after the contact of the reactant solutions and the formation of crystals sediment earlier. Consequently, they cover a larger area within the periphery of the pattern. However, if the concentration of the reactants is lower, the reaction is slower and the precipitate sediments only later. Thus, the forming crystals are located closer to the periphery of the pattern at the end of the flow. In contrast, in the case of calcium–magnesium–carbonate system, the area of precipitate does not change significantly. This is caused by the stoichiometric excess of overall alkaline earth metal concentration compared to the carbonate ions, which is already 1.17 : 1 at the lowest added calcium ion concentration (0.25 M). Therefore, the amount of sodium carbonate is the limiting factor during the experiments. In the case of calcium–magnesium–carbonate system, the grayscale intensity is larger compared to the calcium–carbonate system, which means that there is a slightly greater amount of precipitate. Furthermore, the intensity of the composite pattern does not show significant changes in the measurable calcium ion concentration range.

3.2 Microscopic precipitate characteristics

During the macroscopic characterization of the various composite precipitate patterns, we assumed that the forming alkaline earth metal and magnesium precipitates build up together the precipitate tubes, *i.e.*, mixed precipitates are obtained. To prove this, the same experiments were carried out under an optical microscope (Nikon Eclipse Ts2R coupled with a digital camera). We attempted to examine the microstructure (*i.e.*, morphology) of the precipitate membrane and also the homogeneous (precipitate-filled) parts of the patterns. Images of the crystals were taken at different magnifications (4×, 10×, 20×). In most experiments, the crystals were too small to observe them separately, thus we could not obtain information about the morphology of the crystals that build up the different segments. However, we could identify, which reactant concentrations were beneficial for the formation of precipitate membrane which resulted in tubular structure. We assumed the existence of membrane structure where only a small amount of precipitate was present behind the leading edge of the growing pattern. Therefore, we took the images with the optical microscope from this part of the patterns which is represented in Fig. S3 (ESI†). At lower concentrations we can observe an area without much precipitate inside the macroscopic patterns (images of the 0.25 M column in Fig. 4). On the one hand, the flow carries away the forming crystals, thus they cannot sediment. On the other hand, a thin layer of precipitate could form as well. The microscopic examination revealed that only a few and separated crystals are present in this part of the pattern (Fig. S3 first column, ESI†). Since these crystals are located far from each other, the van der Waals interaction is not possible between them, thus the precipitate membrane cannot form. Contrary to this, in the case of higher concentrations, where the precipitate tube structure was assumed from the macroscopic images (marked parts of the images of 1.00 M column in Fig. 4), we can see that a large amount of small crystals is located very close to each other and due to the interaction between them, they create a membrane structure (wrinkles visible on the

images of the 1.00 M column in Fig. S3, ESI†). The membrane is built up of precipitate bands, whose characteristics depend on the quality and quantity of the added alkaline earth metal ions. Optical microscope images show that, in the case of strontium–magnesium–carbonate system, the increasing concentration results in a stronger precipitate band structure. The increasing concentration of strontium ions causes larger number of crystals, thus each band forms by the interaction of numerous particles. Opposed to this, in the case of calcium–magnesium–carbonate system, this tendency seems to decrease at the highest concentration. The explanation for this is probably that in the case of such concentrated solutions, very strong precipitate wall forms which prevents the further mixing between the reactant solutions. Hence, on the macroscopic precipitate pattern at 1.5 M calcium ion concentration (image of the 1.5 M column in Fig. 4) there is unreacted sodium carbonate solution within the membrane. Thanks to the injection, this sodium carbonate solution pushes forward the formed precipitate wall, and further formation of the precipitate only occurs if the membrane breaks and the mixing between the reactant solutions becomes possible again.

In order to gain more information about the morphology of the crystals, we also examined the microstructure by using a scanning electron microscope (SEM). We were interested in, whether the morphology of the different alkaline earth metal–carbonate crystals changes if the precipitate formation took place in the presence of magnesium ions. To compare the morphology of the crystals obtained in the pure and composite systems, we only examined the dense segment of the patterns by SEM, since the membrane structure was not typical for all pure precipitate patterns. The influence of magnesium ions is presented with SEM images in Fig. 5a. In the top row we can see the samples where the initial calcium, strontium, and barium chloride solutions (0.5 M) did not contain magnesium chloride, while the bottom row shows the samples where the different alkaline earth metal ions were added into a 1.5 M magnesium chloride solution in the same concentration as in the top row. The morphology clearly changes when the system contains two alkaline earth metals at the same time; the presence of magnesium influences the formation of the crystals.[24,25] In the pure calcium–carbonate system, the rhombohedral calcite polymorph is obtained. The presence of the magnesium ions results in a lens-like structure. The irregular shape of crystals in the strontium–carbonate system disappears upon the addition of magnesium ions. In this composite system the crystals show a regular sphere morphology. In contrast to this, in the case of barium–carbonate system, the stick-like crystals become irregular if the system contains magnesium as well. This observation was also confirmed by powder X-ray diffraction (PXRD), and the results for the flow-driven experiments are shown on the example of barium containing system in Fig. 5b-I, III and V. By comparing the characteristic diffractions of barium carbonate crystals with the literature, we found that phase pure crystals were produced in the applied confined flow reactor (Fig. 5b-I).[21] However, in the case of the magnesium containing system, amorphous material formed according to the X-ray

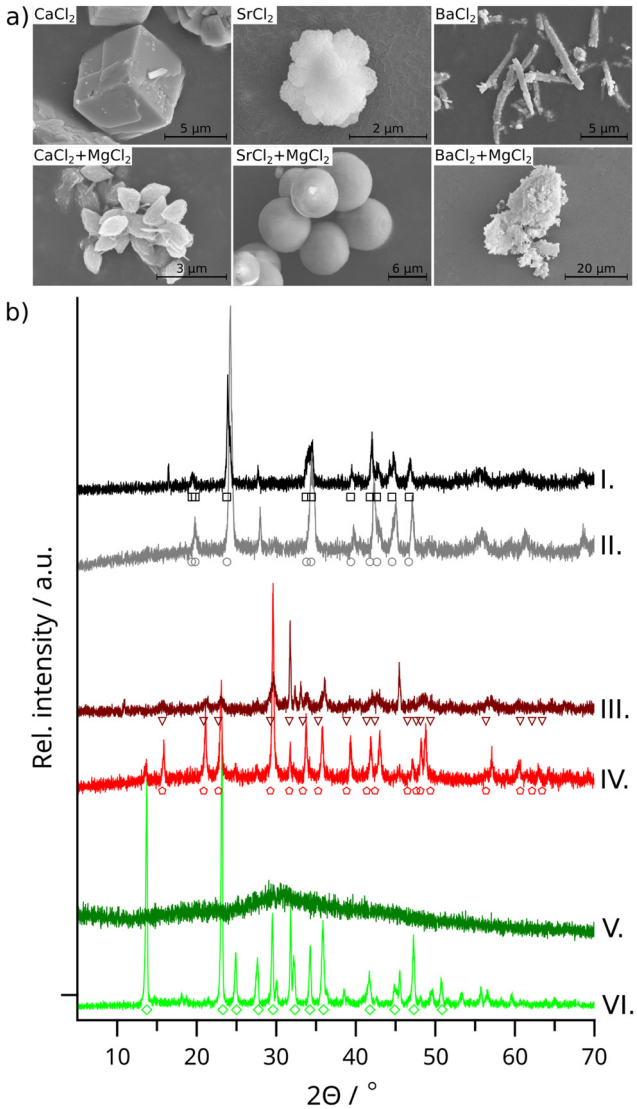

Fig. 5 (a) SEM images representing the morphology of the forming crystals which were present in the different macroscopic precipitate patterns. Top row: systems containing one type of alkaline earth metal (c = 0.5 M); bottom row: magnesium (c = 1.5 M)–carbonate systems doped with alkaline earth metal ions (c = 0.5 M). (b) Powder X-ray diffractograms of pure barium–carbonate system in flow-driven (I) and well-stirred (II) medium, composite barium–magnesium–carbonate system in flow-driven (III) and well-stirred (IV) medium, and magnesium-containing precipitate in flow-driven (V) and well-stirred (VI) medium. Symbols below the diffractograms correspond to published diffractions of various precipitates;[21–23] see Table S1 (ESI†) for more information. $c_{Na_2CO_3}$ = c_{MgCl_2} = 1.5 M; Q = 1 mL min^{-1}; $V_{Na_2CO_3}$ = 5 mL.

diffractogram (Fig. 5b-V). The reason for this could be that this reaction is significantly slower than other alkaline earth metal–carbonate systems, and thus the time scale of the flow is not long enough for the formation of a properly crystallized product. The phase of the composite barium–magnesium–carbonate crystals was determined by using the freely available POW-COD PXRD database.[26] According to the obtained characteristic diffractions (Fig. 5b-III), these crystals were identified as norsethite ($BaMg(CO_3)_2$) mineral,[22] which confirms that the

different ions build up together the composite crystals and result in a new material, which does not resemble any pure carbonate precipitate. Consequently, the presence of magnesium affects both the morphology and the phase of the crystals.

In order to corroborate the above PXRD results, we also performed reference experiments. During these measurements, the synthesis of pure and composite crystals was carried out in well-stirred beakers. In the case of the barium containing system (Fig. 5b-II, IV and VI) it is observed that, the degree of crystallinity is higher when the synthesis happens in a well-stirred system rather than in the flow. Furthermore, some characteristic diffractions appear in the pure magnesium–carbonate system as well (Fig. 5b-VI). In these experiments, the reactant solutions were stirred for 1 hour in 1 : 1 volume ratio, which allowed the formation of a crystalline product. By comparing the characteristic diffractions of these magnesium containing crystals to the literature, the final product of the reaction was identified as nesquehonite ($MgCO_3 \cdot 3H_2O$).[23] However, in the case of the pure barium–carbonate and composite barium–magnesium–carbonate systems, the same product was formed under well-stirred and flow-driven conditions as well (Fig. 5b-II and IV). A new material forms in the composite barium–magnesium–carbonate system, which contains both metal ions together and the PXRD diffractions of this product do not resemble any pure carbonate precipitate.

Compared to the barium-containing flow-driven system, in the case of the composite strontium–magnesium–carbonate (Fig. S4a-III, ESI†) the degree of crystallinity is lower. Furthermore, in the case of the composite calcium–magnesium–carbonate precipitate (Fig. S4b-III, ESI†), only amorphous material forms in the flow-driven experiments. Based on the X-ray diffractions of these products, we could not identify the formed materials. The reactions are slower on going from the barium–magnesium–carbonate system to the calcium–magnesium–carbonate system; therefore, the crystalline product cannot form during the timescale of the flow. In order to collect information about the crystalline phase of these composite systems, we again performed reference experiments in well-stirred beakers (Fig. S4a-II, IV, VI and S4b-II, IV, VI, ESI†). Based on the PXRD diffractograms of the obtained composite crystals, we found that mixed phases formed thanks to the presence of the two metal ions. The product depicts the characteristic diffractions of both pure magnesium- and strontium–carbonate system, and pure magnesium- and calcium–carbonate system.[21,23,27,28] This proves that complex product was produced in calcium and strontium containing systems as well, which explains the change in morphology compared to mono-metallic carbonate systems.

Based on the SEM images, the size of the crystals was also determined in the case of the different alkaline earth metal–carbonate precipitate patterns. We examined how the crystal size depends on the modified composition and concentration. To observe the crystal size evolution, samples of the different patterns were taken through the sealable openings (Fig. 1a) at the same positions. The evaluation was carried out in the ImageJ program and the results are summarized in Table S4 (ESI†). We compared the size of crystals gathered from the different segments (membranous, where the precipitate tube is observed, and dense, where a large amount of separated crystals are present) of alkaline earth metal–carbonate precipitate patterns which were produced at different compositions. When the precipitates contain the different alkaline earth metals individually, the size of the crystals decreases as the concentration increases (top panel of Table S4, ESI†). The reason for this is that the crystal growth process is less favored over nucleation due to the increasing supersaturation. When the precipitates contain magnesium as well, the change in the size shows a partially different trend (lower panel of Table S4, ESI†). In the membranous segment of the patterns the same trend is experienced as described above for the individual systems. However, in the dense part of the pattern, the crystal size rather increases with the increasing concentration, which is unusual. A possible explanation for the latter is that the membrane structure occupies a significant area in the composite precipitate patterns at high concentrations (Fig. 4). As a result, the extent of mixing between the reactant solutions, and thus the supersaturation decreases behind the precipitation front. This favors the crystal growth process and suppresses nucleation. Fig. S5 (ESI†), which was created according to Table S4 (ESI†), illustrates the calcium ion concentration dependence of the crystal size. These samples were taken from the dense part of the patterns. It can be observed that, in the case of the highest calcium chloride concentration (1.5 M), the size of the crystals is the same in the individual and composite patterns. Considering this observation, when the concentration is high enough, the presence of the other ion does not affect the size of the crystals obtained in the alkaline earth metal–carbonate systems, and thus the process of nucleation and crystal growth.

Based on our investigation we can achieve the membrane structure in magnesium–carbonate system as well, if we add another alkaline earth metal of appropriate concentration to the host solution. We were also interested in whether the crystals obtained in the magnesium–carbonate system were involved in the structure of precipitate tubes or only the added alkaline earth metal–carbonate resulted in the membrane structure. In order to investigate this, we prepared element maps by using energy dispersive X-ray spectroscopy (EDX). Fig. 6 shows the element maps in the case of calcium- and strontium–magnesium–carbonate precipitate patterns as an example. According to these results, the particles formed in the magnesium–carbonate system contribute to the tube formation. In addition, the various precipitates crystallize differently in the dense and membranous segments of the patterns. In the membranous segment, the magnesium containing precipitate rather crystallizes separately from the other alkaline earth metals (Fig. 6a and c). In contrast to this, in the dense part of the pattern, the two different ions crystallize together and homogeneous crystals form (Fig. 6b and d). In the membranous segment nucleation is the favored process, while in the dense part the crystal growth is more beneficial. Due to the latter there is enough time for combined precipitate formation.

Finally, we were also interested in whether the composition of the crystals changes according to the stoichiometric ratio of

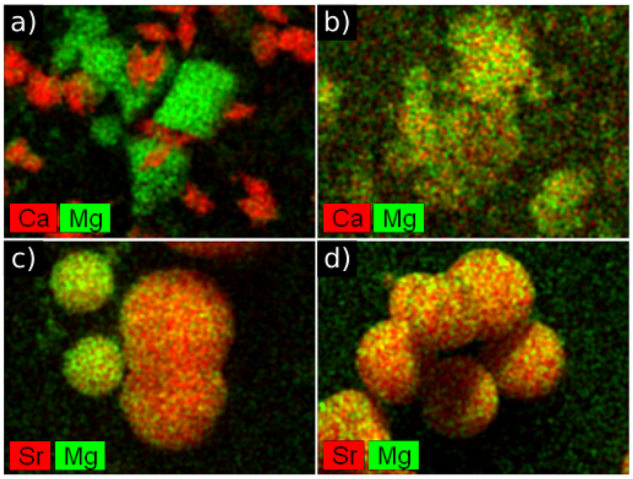

Fig. 6 Artificially colored element map of the crystals obtained in the alkaline earth metal–carbonate systems. Samples were taken from the membranous (a) and (c) and dense (b) and (d) parts of the composite precipitate patterns. c_{CaCl_2} = 0.5 M; c_{SrCl_2} = 0.5 M; $c_{Na_2CO_3}$ = 1.5 M; c_{MgCl_2} = 1.5 M; Q = 1 mL min^{-1}; $V_{Na_2CO_3}$ = 5 mL.

the different metal ions, thus the composition of tubes and dense segments was also determined. Table S5 (ESI†) shows the summary of the elemental composition. Upon examining the amount of calcium, strontium, and barium in the dense segment of the patterns (where the crystals contain the different cations homogeneously), their atomic% grows with their increasing concentration (the concentration of the magnesium chloride is constant, 1.5 M). This growth is consistent with the increase in the stoichiometric excess of alkaline earth metal ions. The cause for this is the difference in the solubility products of precipitates: $pK_{sp,CaCO_3}$ = 8.55, $pK_{sp,SrCO_3}$ = 9.68, $pK_{sp,BaCO_3}$ = 8.29 and $pK_{sp,MgCO_3}$ = 7.46.[29] A lower value of pK_{sp} means a higher solubility of the precipitate. Due to this, by increasing the concentration of the different alkaline earth metals compared to the magnesium, their carbonate containing precipitates displace the magnesium which has the lowest pK_{sp}. In addition, the magnesium–carbonate reaction is slower compared to the other alkaline earth metal–carbonate systems. By examining the amount of the different alkaline earth metals in the membranous segment of the same precipitate patterns, we can observe a discrepancy compared to the dense part. The change of the composition is not consistent with the stoichiometric ratio between the magnesium and the other alkaline earth metals. In the case of calcium and strontium ions, a higher atomic% can be observed than expected at 0.5 M alkaline earth metal concentration. The reason for this could be that, in the membranous segment the crystals crystallize separately (Fig. 6a and c); thus the different crystals appear randomly inside the precipitate tube and in the sample we take.

These results could be of interest if one wants to produce crystals of a desired composition in a similar 2-dimensional flow-driven system. If we apply appropriate conditions, which favor the crystal growth process, we have the possibility to produce composite crystals. In addition, their composition can be influenced by changing the concentration of the reactant solutions as seen in Table S5 (ESI†).

4 Conclusions

We investigated the formation of different alkaline earth metal–carbonate precipitate patterns in a flow-driven system in a confined geometry. We were interested in how the macro- and microstructure (morphology, crystal phase, size, and composition) of precipitate patterns could be influenced by combining different metal ions. During our preliminary experiments it was established that the membrane structure could be produced in the case of all reactants by using appropriate experimental conditions, except for the magnesium–carbonate system. Therefore, we attempted to produce precipitate tubes in the magnesium–carbonate system by adding different alkaline earth metal ions at different concentrations to the magnesium(II) solution. The microstructure of the forming patterns was examined using an optical microscope, SEM, EDX, and PXRD. We found that the precipitate tube structure can be achieved in the magnesium–carbonate system as well, since the added alkaline earth metal ions make nucleation more favored. We also found that the added alkaline earth metal and the magnesium containing precipitates build up together the tubes. The composition and size of these crystals can be influenced by changing the experimental parameters. By fine-tuning the initial concentrations, both well-separated and composite crystals can be produced in which the magnesium and the added alkaline earth metal show a homogeneous distribution. These results show that, by taking advantage of the flow-driven systems and the geometrical benefits of the quasi two dimensional reactor, we can improve the micro- and macrostructure of precipitates by varying the precipitating cations and their concentration ratios.

Author contributions

KB, EB, and GS: conceptualization, investigation, data curation. EB, and GS: writing – original draft. GS: supervision, writing – review & editing.

Conflicts of interest

There are no conflicts to declare.

Acknowledgements

This work was supported by the Ministry of Innovation and Technology of Hungary (TKP2021-NVA-19), and the New National Excellence Program of the Ministry of Culture and Innovation (ÚNKP-22-3-SZTE-387), and from the source of the National Research, Development and Innovation Fund (K138844). E. Balog thanks the ELTE Márton Áron Special College for financial support.

Notes and references

1 J. H. E. Cartwright, J. M. García-Ruiz, M. L. Novella and F. Otálora, Formation of chemical gardens, *J. Colloid Interface Sci.*, 2002, **256**, 351–359.

2 S. Thouvenel-Romans and O. Steinbock, Oscillatory growth of silica tubes in chemical gardens, *J. Am. Chem. Soc.*, 2003, **125**, 4338–4341.
3 J. J. Pagano, S. Thouvenel-Romans and O. Steinbock, Compositional analysis of copper - silica precipitation tubes, *Phys. Chem. Chem. Phys.*, 2007, **9**, 110–116.
4 E. Pópity-Tóth, G. Schuszter, D. Horváth and Á. Tóth, Peristalticity-driven banded chemical garden, *J. Chem. Phys.*, 2018, **148**, 184701.
5 Q. Wang and O. Steinbock, Chemical garden membranes in temperature-controlled microfluidic devices, *Langmuir*, 2021, **37**, 2485–2493.
6 S. Thouvenel-Romans, J. J. Pagano and O. Steinbock, Bubble guidance of tubular growth in reaction-precipitation systems, *Phys. Chem. Chem. Phys.*, 2005, **7**, 2610–2615.
7 L. Roszol and O. Steinbock, Controlling the wall thickness and composition of hollow precipitation tubes, *Phys. Chem. Chem. Phys.*, 2011, **13**, 20100–20103.
8 M. Takiguchi, K. Igarashi, M. Azuma and H. Ooshima, Tubular structure agglomerates of calcium carbonate crystals formed on a cation-exchange membrane, *Cryst. Growth Des.*, 2006, **6**, 1611–1614.
9 K. Igarashi, M. Takiguchi and H. Ooshima, Growth mechanism of the calcium carbonate tubes on a cation-exchange membrane, *JCS-Japan*, 2008, **116**, 111–114.
10 B. Dúzs, I. Lagzi and I. Szalai, Propagating fronts and morphological instabilities in a precipitation reaction, *Langmuir*, 2014, **30**, 5460–5465.
11 E. A. B. Hughes, M. Chipara, T. J. Hall, R. L. Williams and L. M. Grover, Chemobrionic structures in tissue engineering: self-assembling calcium phosphate tubes as cellular scaffolds, *Biomater. Sci.*, 2020, **8**, 812–822.
12 F. Haudin, V. Brasiliense, J. H. E. Cartwright, F. Brau and A. De Wit, Genericity of confined chemical garden patterns with regard to changes in the reactants, *Phys. Chem. Chem. Phys.*, 2015, **17**, 12804–12811.
13 G. Schuszter, F. Brau and A. De Wit, Calcium carbonate mineralization in a confined geometry, *Environ. Sci. Technol. Lett.*, 2016, **3**, 156–159.
14 G. Schuszter and A. De Wit, Comparison of flow-controlled calcium and barium carbonate precipitation patterns, *J. Chem. Phys.*, 2016, **145**, 224201.
15 Q. Wang, K. S. Hernesman and O. Steinbock, *Flow-driven precipitation patterns with microemulsions in a confined geometry, ChemSystemsChem*, 2020, **2**, e1900037.
16 E. Balog, K. Bittmann, K. Schwarzenberger, K. Eckert, A. De Wit and G. Schuszter, Influence of microscopic precipitate structures on macroscopic pattern formation in reactive flows in a confined geometry, *Phys. Chem. Chem. Phys.*, 2019, **21**, 2910–2918.
17 Y. Nagatsu, Y. Ishii, Y. Tada and A. De Wit, Hydrodynamic fingering instability induced by a precipitation reaction, *Phys. Rev. Lett.*, 2014, **113**, 024502.
18 F. Haudin and A. De Wit, Patterns due to an interplay between viscous and precipitation-driven fingering, *Phys. Fluids*, 2015, **27**, 113101.
19 E. Balog, P. Papp, Á. Tóth, D. Horváth and G. Schuszter, The impact of reaction rate on the formation of flow-driven confined precipitate patterns, *Phys. Chem. Chem. Phys.*, 2020, **22**, 13390–13397.
20 N. Prabha Das, R. Zahorán, L. Janovák, Á. Deák, Á. Tóth, D. Horváth and G. Schuszter, Kinetic characterization of precipitation reactions: possible link between a phenomenological equation and reaction pathway, *Cryst. Growth Des.*, 2020, **20**, 7392–7398.
21 L. Chen, J. Jiang, Z. Bao, J. Pan, W. Xu, L. Zhou, Z. Wu and X. Chen, Synthesis of barium and strontium carbonate crystals with unusual morphologies using an organic additive, *Russ. J. Phys. Chem.*, 2013, **87**, 2239–2245.
22 C. Pimentel, C. M. Pina and C. I. Sainz-Díaz, New insights into dolomite and dolomite-analogue structures from first principles calculations, *ACS Earth Space Chem.*, 2022, **6**, 2360–2367.
23 Q. Chen, T. Hui, H. Sun, T. Peng and W. Ding, Synthesis of magnesium carbonate hydrate from natural talc, *Open Chem. J.*, 2020, **18**, 951–961.
24 F. Qing, Principles of Calcium-Based Biomineralization, *prog. Mol. Subcell. Biol.*, 2011, **52**, 141–197.
25 L. Fernandez-Diaz, A. Putnis, M. Prieto and C. V. Putnis, The role of magnesium in the crystallization of calcite and aragonite in a porous medium, *J. Sediment. Res.*, 1996, **66**, 482–491.
26 A. Altomare, N. Corriero, C. Cuocci, A. Falcicchio, A. Moliterni and R. Rizzi, QUALX2.0: a qualitative phase analysis software using the freely available database POW-COD, *J. Appl. Cryst.*, 2015, **48**, 598–603.
27 B. Boudaira, A. Harabi, F. Bouzerara, F. Zenikheri, L. Foughali and A. Guechi, Preparation and characterization of membrane supports for microfiltration and ultrafiltration using kaolin (DD2) and $CaCO_3$, *Desalination Water Treat*, 2016, **57**, 5258–5265.
28 M. C. Reis, M. F. B. Sousa, F. Alobaid, C. A. Bertran and Y. Wang, A two-fluid model for calcium carbonate precipitation in highly supersaturated solutions, *Adv. Powder Technol.*, 2018, **29**, 1571–1581.
29 S. Kotrlý and L. Šu*cha, Handbook of chemical equilibria in analytical chemistry*, Ellis Horwood Limited, England, 1985.